

Determination of visible near-IR absorption coefficients of mammalian fat using time- and spatially resolved diffuse reflectance and transmission spectroscopy

R. L. P. van Veen

H. J. C. M. Sterenberg

Erasmus Medical Center Rotterdam
Center for Optical Diagnostics and Therapy
Department of Radiation Oncology
Westzeedijk 118, 3008 CA
The Netherlands
E-mail: h.j.c.m.sterenberg@erasmusmc.nl

A. Pifferi

A. Torricelli

E. Chikoidze

R. Cubeddu

Politecnico di Milano
Istituto Nazionale per la Fisica della Materia
Dipartimento di Fisica e Istituto di Fotonica
e Nanotecnologie
Consiglio Nazionale delle Ricerche
Piazza Leonardo da Vinci 32
I-20133 Milan, Italy

Abstract. *In-vivo* optical spectroscopy and the determination of tissue absorption and scattering properties have a central role in the development of novel optical diagnostic and therapeutic modalities in medicine. A number of techniques are available for the optical characterization of tissue in the visible near-IR region of the spectrum. An important consideration for many of these techniques is the reliability of the absorption spectrum of the various constituents of tissue. The availability of accurate absorption spectra in the range 600 to 1100 nm may allow for the determination of the concentration of key tissue constituents such as oxy- and deoxy-hemoglobin, water, and lipids. The objective of the current study is the determination of a reliable absorption spectrum of lipid(s) that can be used for component analysis of *in-vivo* spectra. We report the absorption spectrum of a clear purified oil obtained from pig lard. In the liquid phase above 36°C, the oil is transparent and thus suitable for collimated transmission measurements. At room temperature, the oil is a solid grease that is highly scattering. The absorption and scattering properties in this solid phase are measured using time- and spatially resolved diffuse reflectance spectroscopy. Using these three independent measurement techniques, we have determined an accurate estimate for the absorption spectrum of mammalian fat. © 2005 Society of Photo-Optical Instrumentation Engineers. [DOI: 10.1117/1.2085149]

Keywords: visible near-IR; spectroscopy; absorption; scattering; fat.

Paper 04245R received Dec. 17, 2004; revised manuscript received Apr. 12, 2005; accepted for publication Apr. 27, 2005; published online Oct. 10, 2005.

1 Introduction

Near-infrared (NIR) spectroscopic imaging is a relatively new, noninvasive medical diagnostic technique, which may provide several advantages over other diagnostic methods. At present, several groups are investigating different tomographic,^{1,2} multispectral transillumination optical imaging^{3,4} or spectroscopic techniques.⁵ These measurements are performed either by continuous wave, or by time/frequency resolved methods. Contrast between diseased and normal tissues resulting from differences in tissue optical properties, e.g., reduced scattering and absorption coefficients, may be caused by differences (extra or intra) cellular refractive index distributions, variations in blood saturation, and variations in blood, water, or lipid content. Recent work on NIR optical mammography suggests that malignant and benign tissue structures can be discriminated from normal tissue by their water lipid ratios or due to differences in total hemoglobin content and oxygenation. Tumors are associated with an increase in blood volume and a decrease in oxygenation due to tumor proliferation.⁶⁻⁸ The absorption spectra

obtained from these techniques are assumed/thought to be a linear combination of the absorption spectra of the chromophores present in the tissue. Spectral decomposition of the measured absorption spectra into its components can be used to quantify absolute tissue chromophore concentrations. Furthermore, tissue oxygenation and total hemoglobin content can be calculated from these quantities. It is therefore essential to have detailed knowledge of the intrinsic absorption spectra of these four components. Oxy, deoxy-hemoglobin,⁹ and water¹⁰ are well quantified and routinely applied. A representative tissue fat spectrum, however, has yet to be determined. The fat spectra used for spectral decomposition vary between investigators. Heusmann, Kolzer, and Mitic¹¹ employ a nonspecified vegetable oil for the component analysis of the female breast tissue, whereas others have used olive oil,¹² raw pig lard,¹³ sunflower oil,¹⁴ or soybean oil.¹⁵ Other investigators even assume a negligible absorption due to fat. These spectra are significantly different from each other in respect to their spectral shape and the magnitude of the main absorption peaks. This makes an absolute comparison and interpretation of the results of each technique difficult. The reason for the absence of a definitive fat spectrum in the literature is that mammalian fat is not available as a pure clear liquid. We

Address all correspondence to Robert L. P. van Veen, CODT, ErasmusMC/ Rotterdam, westzeedijk 118, Rotterdam, Zuid Holland 3000 CA, Netherlands. Tel: +311104632101. Fax: +311104632141. E-mail: r.vanveen@erasmusmc.nl

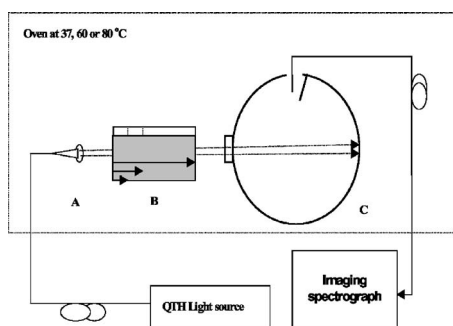


Fig. 1 Schematic outlay of the transmission setup: (a) collimating optics, (b) quartz cuvettes with lengths of 10, 20 or 50 mm, and (c) integrating sphere plus detection fiber. The dotted line indicates the oven used for constant temperatures.

report the absorption spectrum of clear oil obtained from mammalian pig lard. At room temperature, this oil is a solid grease that displays strong scattering properties. Absorption and scattering properties of this solid grease were measured using time- and spatially resolved diffuse reflectance spectroscopy. At temperatures above 36°C, it is a clear liquid with minimal scattering properties. Hence, an independent measurement of the absorption spectrum can be made using collimated transmission measurements.

2 Materials and Methods

2.1 Lipid Purification

5 kg of muscle and skin-free pig chest plate lard was divided in pieces of 1 cm³ and placed in water maintained at a temperature of 90°C. A thin layer of oil formed on the surface of the mixture and was removed and placed in a separate container. This process was continued for a period of 6 h until the oil separation process had stopped. The oil still contained water and other visible tissue structures. The container was then placed in an oven at 50°C to homogenize the fluid, and then was placed in a refrigerator at 5°C. After one hour, the oil had solidified into a pure white solid lipid above a multilayered mixture of water and gelatinous substance. The lipid could then be separated manually from the mixture below. The solid oil was then heated once more to 80°C and passed twice through filter paper (standard grade 91, 10 μm, Whatman International Limited, England) while it remained in its liquid state. The filtered oil was heated again to 80°C and poured onto a filter containing sodium sulphate (Na₂SO₄ Anhydrous J.T. Baker BV, The Netherlands) to remove any remaining water. Finally, the oil was placed in a test tube and centrifuged (Gyro Vap) for 30 min at 1000 rpm at a constant temperature of 70°C. Pure oil was removed using a pipette, leaving some sediment at the base of the test tube. At the end of this process, 250 ml of oil was obtained that was visually clear at temperatures above 36°C.

2.2 Collimated Transmission Measurement

The setup used is shown schematically in Fig. 1. Light from a 100-W quartz tungsten halogen lamp is coupled into an optical fiber leading to a cuvette holder (Avantes, Eerbeek, The Netherlands) and collimated to a beam of approximately 2 mm diam. Three different quartz cuvettes (Anadis, Malden,

The Netherlands) with path lengths of 10, 20, and 50 mm were used. Transmitted light was collected using an integrating sphere with a collection port much larger than the beam diameter (Oriel Instruments, Stratford, Connecticut). In this way, divergence of the light beam within cuvettes of different path length did not affect the total amount of light collected. The detection fiber was positioned inside the integrating sphere behind a baffle and directed the collected light to the entrance slit position of an imaging spectrograph (Oriel, MS257). It was spectrally projected onto a 16-bit 256 to 1024 pixel CCD camera cooled to -30 °C (Andor DU420-OE, Belfast, Northern Ireland). The 150-lines/mm grating in the spectrograph allows us to cover a wavelength range from 440 to 1100 nm with a spectral resolution of 0.65 nm. The cuvette holder and integrating sphere were placed in an oven, and optical fibers were passed between the rubber fitting of the oven door to the spectrograph. Measurements were performed at constant temperatures of 37, 60, and 80 °C. To avoid possible temperature gradient effects, the setup was allowed to settle for at least 20 min at each temperature setting. For each cuvette path length, three sequential transmission and background measurements were performed.

The transmission data were averaged over the three sequential measurements and the background was subtracted. The absorption coefficients were calculated for three path length differences (50 to 10, 50 to 20, and 20 to 10 mm) according to Eq. (1).

$$\mu_{a,\text{meas}}(\lambda) = \frac{\left\{ \left[\frac{LN(I_{10}/I_{50})}{d_{50} - d_{10}} \right] + \left[\frac{LN(I_{20}/I_{50})}{d_{50} - d_{20}} \right] + \left[\frac{LN(I_{10}/I_{20})}{d_{20} - d_{10}} \right] \right\}}{3}, \quad (1)$$

where $I_{10,20, \text{ and } 50}$ is the measured transmission intensity in CCD counts for the three cuvettes path lengths $d_{50,40, \text{ and } 10}$ mm. The use of this method makes reference measurements, i.e., empty cuvette or water, obsolete, thus the absorption information originates solely from the transmission differences between the three path lengths and excludes all cuvette / oil boundary reflection effects. Second, the use of small path lengths and longer path lengths, e.g., 10 and 40 mm, provides accurate spectral information in regions of low and high absorption coefficients, respectively. Absorption coefficients were calculated for all three temperatures (37, 60, and 80 °C) to investigate the possible influence of temperature on the absorption coefficient.

2.3 Spatially Resolved Diffuse Reflectance Spectroscopy

The measurement technique is based on a theoretical analysis developed by Farrell, Patterson, and Wilson.¹⁶ The illumination of the solid fat and the collection of the diffuse re-emitted light were performed by a multifiber probe. This black Perspex probe consists of 10 low OH medical grade fibers (400-μm core, length of about 4 m, CeramOptec GmbH, Bonn, Germany, in which the fibers are positioned at an average interfiber distance of 2 mm. The white light from a 100-W quartz tungsten halogen lamp is coupled into the illu-

mination fiber of the probe. The nine detection fibers in the probe direct the light to the entrance slit position of an imaging spectrograph (Oriel, MS257). The 150-lines/mm grating in the spectrograph allows us to cover a wavelength range from 600 to 1100 nm with a spectral resolution of 0.65 nm. A 16-bit 256 to 1024 pixel CCD camera cooled to 30°C (Andor DU420-OE, Belfast Northern Ireland) detects the nine spectra originating at different distances from the illumination fiber. The solid fat was placed in a container, and the sample dimensions were $8 \times 8 \times 5$ cm. Three measurements were taken at room temperature at three different positions on the sample.

Data processing and analyses of the data files were performed using Matlab software (Matlab, Mathworks Incorporated, Natick, Massachusetts). Absorption and scattering spectra were obtained by fitting the diffusion equation and assuming Lorentz-Mie scattering according to Eq. (2) for all wavelengths.

$$\mu'_s = a \cdot \lambda^{-b}, \quad (2)$$

where b is a constant and is related to the size of the scattering particles. Further details on the fit method can be found in Refs. 14 and 17.

2.4 Time-Resolved Diffuse Reflectance Spectroscopy

The measurement setup consists in a fully automated system for time-resolved reflectance spectroscopy continuously tunable in the 610 to 1050 nm range.¹³ A synchronously pumped mode-locked dye (DCM) laser was used as the excitation source from 610 to 700 nm, while an actively mode-locked titanium:sapphire laser provided light in the wavelength range of 705 to 1050 nm. A couple of 1-mm plastic glass fibers (PCS1000W, Quartz et Silice, France) delivered light into the sample and collected the reflected photons at a relative distance of 1.5 cm. A double microchannel plate photomultiplier (R1564U with S1 photocathode, Hamamatsu, Japan) and a PC board for time-correlated single-photon counting (SPC134, Becker and Hickl, Germany) were used for detection. A small fraction of the incident beam was coupled to a 1-mm fiber (PCS1000W, Quartz et Silice, France) and fed directly to the photomultiplier to account for on-line recording of the instrumental response function (IRF). Overall, the IRF was <120 and <180 ps FWHM in the red and near-infrared, respectively. Time-resolved reflectance curves were collected every 5 nm with an acquisition time of 4 s for each wavelength.

The reduced scattering and absorption spectra were constructed by plotting, versus wavelength, the values of μ'_s and μ_a , as obtained from fitting the experimental data with a standard solution of the diffusion approximation to the transport equation for a semi-infinite homogeneous medium¹⁸ using the extrapolated boundary condition.¹⁹ The diffusion coefficient D was taken to be independent of the absorption properties of the medium [i.e., $D=1/(3\mu'_s)$], in agreement with Furutsu and Yamada.²⁰ The theoretical curve was convoluted with the IRF and normalized to the area of the experimental curve. The fitting range included all points with a number of counts higher than 80% of the peak value on the rising edge of the curve and 1% on the tail. The best fit was reached with a Levenberg-Marquardt algorithm²¹ by varying both μ'_s and μ_a to minimize the reduced χ^2 .

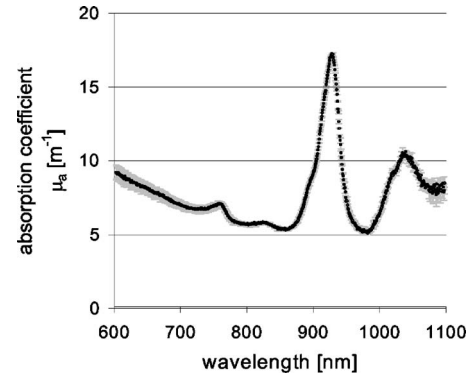


Fig. 2 Example of absorption coefficients plus scattering contribution versus wavelength of liquid pig oil at 60°C, calculated according to Eq. (1). Error bars represent the standard deviation over the average of the three different path lengths (10, 20, and 50 mm).

The exact temporal position of the IRF (t_0) was obtained fitting the experimental curves in the region of low absorption with the three free parameters μ'_s , μ_a , and t_0 .²² The average value of t_0 was then applied as a fixed parameter to all wavelengths.

In the range of measured values of the optical coefficients, with our setup and the theoretical model we use, the accuracy in the absolute estimate of both μ'_s and μ_a is usually better than 10%.^{22,23}

3 Results

Figure 2 shows the results of the transmission measurements at 60°C calculated according to Eq. (1). The results for 37°C were similar. Although the oil sample was visually clear, some scattering could be observed as the light beam was visible from the side of the cuvette, indicating the presence of some remaining scattering particles. As seen in Fig. 2, the absorption spectrum appears to be superimposed on Mie-like scattering. An initial analysis revealed six major absorption peaks. Five peaks consisted of two nearly coinciding absorption bands. The result at 80°C clearly shows a much lower scattering contribution. To eliminate the Mie-like scattering contribution from the absorption coefficient, we fitted 11 Gaussian-shaped absorption peaks plus a Mie-like scattering function through the transmission result, as shown in Eq. (3), for all three temperatures separately.

$$\mu_{a \text{ model}} = A \cdot \exp \left[-B \cdot \text{LN} \left(\frac{\lambda}{\lambda_0} \right) \right] + \sum_i C_i \cdot \exp \left[- \left(\frac{\lambda_i - \lambda}{\sigma_i} \right)^2 \right], \quad (3)$$

where in the first term, the scattering contribution is defined by A and B , respectively related to scatter size and density, and λ_0 is the central fit wavelength. In the second term, the summation of the 11 absorption Gaussians is where C_i represents the absorption magnitude, λ_i the center peak wavelength, and σ_i the bandwidth of each absorption band, indicated with i . Fit constraints were non-negative fit parameters and absorption coefficient results. The scattering spectrum re-

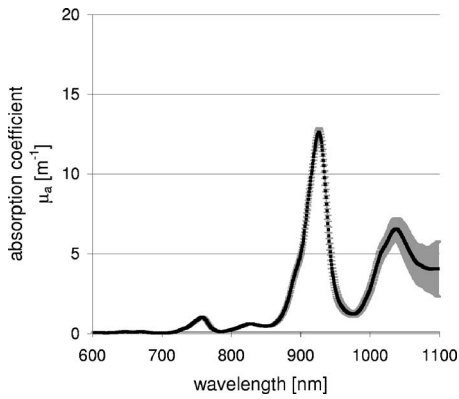


Fig. 3 Absorption coefficient after correction for scattering contribution versus wavelength. The error bars represent the standard deviation over the three temperatures, i.e., 37, 60, and 80 °C.

sulting from the fit was then subtracted from the original absorption spectrum results to obtain the absolute absorption coefficients. The average absorption coefficients at 37, 60, and 80 °C are shown in Fig. 3. Absorption spectra of all three temperatures coincide from 600 up to 980 nm. Above 980 nm and higher, the absorption coefficients of the measurement at 80°C become up to 25% smaller compared to 37 and 60 °C. The relative error for each temperature, between the model and measurement, was within 5% over the entire wavelength interval (600 up to 1100 nm). Values found for the scatter slope ($-b$) ranged from 1.7 up to 2.6, indicating Lorentz-Mie scattering.

Figure 4 shows the absorption (μ_a) spectrum of the solidified lipid sample obtained after averaging three relocated sequential spatially resolved diffuse reflectance spectroscopy (DRS) measurements performed at 15°C. The main absorption peak is located at 930 nm (15.7 m^{-1}) with an overtone at 760 nm (1.47 m^{-1}). Reduced scattering properties decreased as function of wavelength ($\mu'_s = 654 \text{ m}^{-1}$ at 600 nm down to 370 m^{-1} at 1087 nm).

Figure 5 shows the absorption (μ_a) spectrum of the purified lipid sample obtained averaging three consecutive spec-

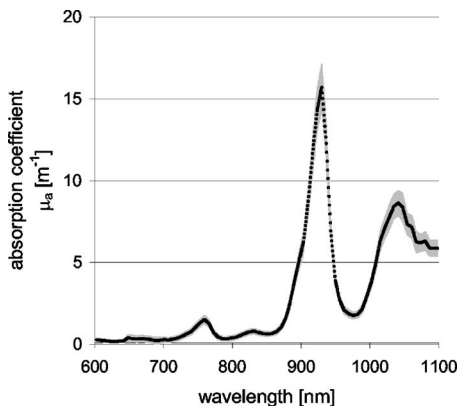


Fig. 4 Absorption coefficient versus wavelength of pig oil at 15°C in solid state resulting from the spatially resolved measurements with a 0.65-nm resolution. The error bars represent the standard deviation over the three sequential measurements after repositioning.

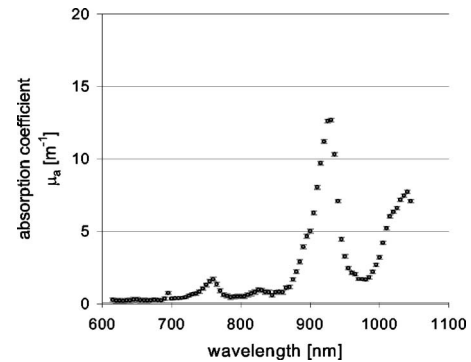


Fig. 5 Absorption coefficient versus wavelength of pig oil at 15°C in solid state resulting from the time-resolved measurements with a 5-nm resolution. The error bars represent the standard deviation over the three sequential measurements after repositioning.

tral time-resolved DRS acquisitions performed at 15°C. The absorption spectrum shows two major peaks at 930 nm (12.8 m^{-1}), and at 760 nm (1.73 m^{-1}), while the peak around 1044 nm is beyond the tuning range of the instrumentation. The reduced scattering coefficient is a decreasing function of wavelength with values in the range 700 to 450 m^{-1} . As for the DRS, on increasing the sample temperature from 0 to 25°C, as expected we observed a progressive decrease of μ'_s (data not shown). The data presented in Fig. 5 correspond to the highest temperature at which the scattering coefficient is high enough to provide fully reliable results.²² Up to this temperature, no significant variations were observed in the absorption spectrum (data not shown).

In Fig. 6, the spectra of all three techniques are shown in log scale to illustrate spectral features at low absorption. Table 1 gives an overview on the main spectral absorption features as measured by all three techniques, plus the average of all three methods.

4 Discussion and Conclusions

We present the absorption spectrum of mammalian fat measured by three independent methods. Direct measurement on pig lard to obtain optical properties of mammalian fat was not feasible, because this adipose tissue still contains blood and water. Transmission measurement of visually clear lard oil

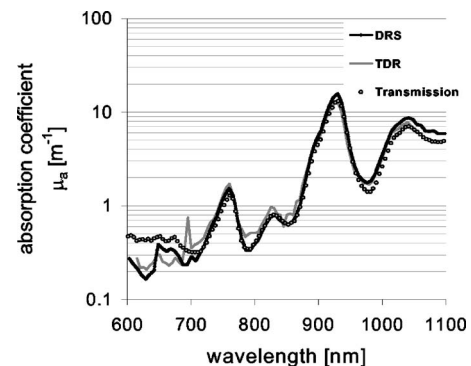


Fig. 6 Absorption coefficient versus wavelength of mammalian fat in solid and liquid state, resulting from the time/spatially resolved and transmittance measurements.

Table 1 Main absorption peaks characteristics between 600 up to 1100 nm of mammalian fat for all three techniques. The average of all three techniques is given in the last column.

λ [nm]	Transmittance	SD	DRS	SD	TR	SD	Average
670.4	0.45	0.15	0.34	0.20	0.25	0.26	0.35
760.2	1.28	0.21	1.50	0.25	1.70	0.10	1.49
830.7	0.80	0.17	0.80	0.17	0.95	0.07	0.85
929	13.10	0.26	15.69	1.42	12.7	0.36	13.80
1040	7.02	0.13	8.62	0.75	7.74	0.04	7.78

still contained some scattering. The result at 80°C clearly shows a much lower scattering contribution, suggesting that the scattering observed is related to microscopic traces of solidification at the lower temperatures or changes in shape/mixture of fat partitions in the liquid fat rather than impurities. A maximal amount of Mie-like scattering was subtracted from the attenuation data, as seen in Figs. 2 and 3, due to the employed fit constraints. Despite the good fit results, some uncertainty still remains regarding the absolute amount of scattering subtracted. The absorption coefficients determined at 80°C become smaller at wavelengths higher than 980 nm and may reflect temperature dependence of the absorption.

The results of the time- and spatially resolved measurement reveal less spectral information at lower wavelengths. For DRS, this may indicate insufficient capacity to uncouple scattering from absorption, especially for low absorption. Concerning the time-resolved spectroscopy (TRS) data, the measurement performed to very low absorption (i.e., <700 nm), is possibly affected by the problem of pile-up of time-resolved photon distributions due to the long decay time associated with low μ_a . The data presented were obtained applying background subtraction at the experimental curves that can result in a slight overestimation of the absorption coefficient. To demonstrate the differences in absorbing properties between the several types of oil, we have measured the absorption of cod liver, mineral, and soya oil. Measurements were performed using a standard transmission method. The results are depicted in Fig. 7. All three spectra show a mod-

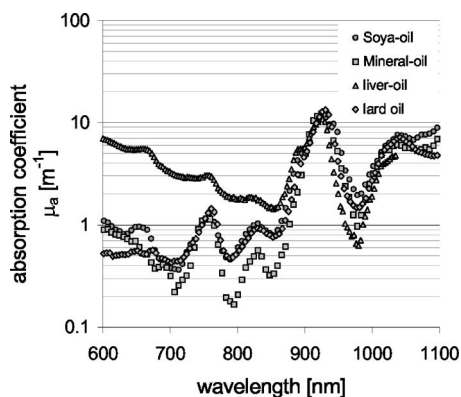


Fig. 7 Absorption coefficient versus wavelength of pig lard oil (solid line), soya oil (filled circle), mineral oil (filled squares), and cod liver oil (filled triangles).

erate scattering slope from approximately 600 up to 700 nm and small differences in spectral shape, and may contain chlorophyll. Furthermore, differences in absorption are observed. Using one of these spectra in a component analysis of absorption spectra may therefore result in differences in absolute chromophore concentration. In summary, we determine the absorption spectrum of mammalian oil validated using three independent techniques. Incorporation of standard intrinsic absorption spectra enables a more reliable comparison between techniques and methods used in NIR spectroscopy for the analysis of absolute tissue chromophore content.

Acknowledgments

The work was partially funded by the European Union Center for Ultra-fast Science and Biomedical Optics (CUSBO contract HPRI-CT-2001-00148) and by the European Union Projects Medphot (contract QLG1_CT-2000-01464) and Optimamm (contract QLG1_CT-2000-00690). Furthermore, we would like to thank the Department of Pharmacology for their suggestions and assistance, and Scott Prahl of the Oregon Medical Laser Center for placing spectrum and data on their web site (<http://omlc.ogi.edu/spectra/>).

References

1. J. C. Hebden, H. Veenstra, H. Dehghani, E. M. Hillman, M. Schweiger, S. R. Arridge, and D. T. Delpy, "Three-dimensional time-resolved optical tomography of a conical breast phantom," *Appl. Opt.* **40**, 3278–3287 (2001).
2. B. W. Pogue, S. P. Poplack, T. O. McBride, W. A. Wells, K. S. Osterman, U. L. Osterberg, and K. D. Paulsen, "Quantitative hemoglobin tomography with diffuse near-infrared spectroscopy: Pilot results in the breast," *Radiology* **218**, 261–266 (2001).
3. A. Pifferi, P. Taroni, A. Torricelli, F. Messina, R. Cubeddu, and G. Danesini, "Four-wavelength time-resolved optical mammography in the 680–980-nm range," *Opt. Lett.* **28**, 1138–1140 (2003).
4. D. Grosenick, K. T. Moesta, H. Wabnitz, J. Mucke, C. Stroszczynski, R. Macdonald, P. M. Schlag, and H. Rinneberg, "Time-domain optical mammography: Initial clinical results on detection and characterization of breast tumors," *Appl. Opt.* **42**, 3170–3186 (2003).
5. N. Shah, A. Cerussi, C. Eker, J. Espinoza, J. Butler, J. Fishkin, R. Hornung, and B. Tromberg, "Noninvasive functional optical spectroscopy of human breast tissue," *Proc. Natl. Acad. Sci. U.S.A.* **98**, 4420–4425 (2001).
6. B. J. Tromberg, O. Coquoz, J. B. Fishkin, T. Pham, E. R. Anderson, J. Butler, M. Cahn, J. D. Gross, V. Venugopalan, and D. Pham, "Non-invasive measurements of breast tissue optical properties using frequency-domain photon migration," *Philos. Trans. R. Soc. London, Ser. B* **352**, 661–668 (1997).
7. S. Thomsen and D. Tatman, "Physiological and pathological factors of human breast disease that can influence optical diagnosis," *Ann. N.Y. Acad. Sci.* **838**, 171–193 (1998).

8. B. Beauvoit, T. Kitai, and B. Chance, "Contribution of the mitochondrial compartment to the optical properties of the rat liver: A theoretical and practical approach," *Biophys. J.* **67**, 2501–2510 (1994).
9. S. J. Matcher, C. E. Elwell, C. E. Cooper, M. Cope, and D. T. Delpy, "Performance comparison of several published tissue near-infrared spectroscopy algorithms," *Anal. Biochem.* **227**, 54–68 (1995).
10. G. M. Hale and M. R. Querry, "Optical constants of water in the 200-nm to 200-micrometer wavelength region," *Appl. Opt.* **12**, 555–563 (1973).
11. H. Heusmann, J. Kolzer, and G. Mitic, "Characterization of female breast in vivo by time resolved and spectroscopic measurements in near infrared spectroscopy," *J. Biomed. Opt.* **1**, 425–434 (1996).
12. V. Quaresima, S. J. Matcher, and M. Ferrari, "Identification and quantification of intrinsic optical contrast for near-infrared mammography," *Photochem. Photobiol.* **67**, 4–14 (1998).
13. A. Torricelli, A. Pifferi, P. Taroni, E. Giambattistelli, and R. Cubeddu, "In vivo optical characterization of human tissues from 610 to 1010 nm by time-resolved reflectance spectroscopy," *Phys. Med. Biol.* **46**, 2227–2237 (2001).
14. R. L. P. van Veen, W. Verkruijsse, and H. J. C. M. Sterenborg, "Diffuse reflectance spectroscopy from 500 to 1060 nm by correction for inhomogeneously distributed absorbers," *Opt. Lett.* **27**, 246–248 (2002).
15. A. E. Cerussi, D. Jakubowski, N. Shah, F. Bevilacqua, R. Lanning, A. J. Berger, D. Hsiang, J. Butler, R. F. Holcombe, and B. J. Tromberg, "Spectroscopy enhances the information content of optical mammography," *J. Biomed. Opt.* **7**, 60–71 (2002).
16. T. J. Farrell, M. S. Patterson, and B. Wilson, "A diffusion theory model of spatially resolved, steady-state diffuse reflectance for the noninvasive determination of tissue optical properties in vivo," *Med. Phys.* **19**, 879–888 (1992).
17. R. M. P. Doornbos, R. Lang, F. W. Cross, and H. J. C. M. Sterenborg, "The determination of in-vivo human tissue optical properties and absolute chromophore concentrations using spatially resolved steady state diffuse reflectance spectroscopy," *Phys. Med. Biol.* **44**, 967–981 (1999).
18. M. S. Patterson, B. Chance, and B. C. Wilson, "Time resolved reflectance and transmittance for the non invasive measurement of tissue optical properties," *Appl. Opt.* **28**, 2331–2336 (1989).
19. R. C. Haskell, L. O. Svasaand, T. T. Tsay, T. C. Feng, M. S. McAdams, and B. J. Tromberg, "Boundary conditions for the diffusion equation in radiative transfer," *J. Opt. Soc. Am. A* **11**, 2727–2741 (1994).
20. K. Furutsu and Y. Yamada, "Diffusion approximation for a dissipative random medium and the applications," *Phys. Rev. E* **50**, 3634–3640 (1994).
21. W. H. Press, S. A. Teukolsky, W. T. Vetterling, and B. P. Flannery, *Numerical Recipes in C: The Art of Scientific Computing*, Cambridge University Press, New York (1992).
22. R. Cubeddu, A. Pifferi, P. Taroni, A. Torricelli, and G. Valentini, "Experimental test of theoretical models for time-resolved reflectance," *Med. Phys.* **23**, 1625–1633 (1996).
23. R. Cubeddu, M. Musolino, A. Pifferi, P. Taroni, and G. Valentini, "Time-resolved reflectance: a systematic study for the application to the optical characterisation of tissue," *IEEE J. Quantum Electron.* **30**, 2421–2430 (1994).